Experimental study of the series resistance effect and its impact on the compact modeling of the conduction characteristics of HfO$_2$-based resistive switching memories

EP

D. Maldonado, F. Aguirre, G. González-Cordero, A. M. Roldán, M. B. González, F. Jiménez-Molinos, F. Campabadal, E. Miranda, J. B. Roldán, et al.

COLLECTIONS

EP   This paper was selected as an Editor's Pick

View Online   Export Citation   CrossMark

ARTICLES YOU MAY BE INTERESTED IN

Origin of the high-temperature ferromagnetism in Co-doped PbPdO$_2$ semiconductors: A theoretical and experimental study
Journal of Applied Physics **130**, 055705 (2021); https://doi.org/10.1063/5.0057491

Impact of the nucleation of conducting clusters on the retention of memristors: A self-consistent phase-field computational study
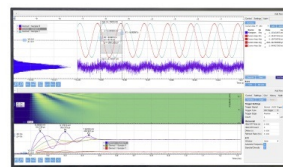Journal of Applied Physics **130**, 054901 (2021); https://doi.org/10.1063/5.0055083

New method of transport measurements on van der Waals heterostructures under pressure
Journal of Applied Physics **130**, 064303 (2021); https://doi.org/10.1063/5.0058583

Experimental study of the series resistance effect and its impact on the compact modeling of the conduction characteristics of HfO$_2$-based resistive switching memories EP

D. Maldonado,[1] 🆔 F. Aguirre,[2,3,4] 🆔 G. González-Cordero,[1] 🆔 A. M. Roldán,[1] 🆔 M. B. González,[5] 🆔
F. Jiménez-Molinos,[1] 🆔 F. Campabadal,[5] 🆔 E. Miranda,[4] 🆔 and J. B. Roldán[1,a] 🆔

AFFILIATIONS

[1]Departamento de Electrónica y Tecnología de Computadores, Universidad de Granada, Facultad de Ciencias, Avd. Fuentenueva s/n, 18071 Granada, Spain
[2]Unidad de Investigación y Desarrollo de las Ingenierías (UIDI), Facultad Regional Buenos Aires, Universidad Tecnológica Nacional, Medrano 951 (C1179AAQ), Buenos Aires, Argentina
[3]Consejo Nacional de Investigaciones Científicas y Técnicas (CONICET), Godoy Cruz 2290 (C1425FQB), Buenos Aires, Argentina
[4]Deparment d'Enginyeria Electrònica, Universitat Autònoma de Barcelona, Edifici Q. 08193 Bellaterra, Spain
[5]Institut de Microelectrònica de Barcelona, IMB-CNM (CSIC), Carrer dels Til·lers, s/n. Campus UAB, 08193 Bellaterra, Spain

[a]Author to whom correspondence should be addressed: jroldan@ugr.es

ABSTRACT

The relevance of the intrinsic series resistance effect in the context of resistive random access memory (RRAM) compact modeling is investigated. This resistance notably affects the conduction characteristic of resistive switching memories so that it becomes an essential factor to consider when fitting experimental data, especially those coming from devices exhibiting the so-called snapback and snapforward effects. A thorough description of the resistance value extraction procedure and an analysis of the connection of this value with the set and reset transition voltages in HfO$_2$-based valence change memories are presented. Furthermore, in order to illustrate the importance of this feature in the shape of the I–V curve, the Stanford model for RRAM devices is enhanced by incorporating the series resistance as an additional parameter in the Verilog-A model script.

I. INTRODUCTION

Resistive Random Access Memories (RRAMs) are nowadays under study worldwide for their outstanding potential in the development of non-volatile memory-based applications.[1,2] Because of their tunable conduction properties, resistive switching devices are also gaining momentum in the neuromorphic circuit landscape since they can mimic biological synapses.[3–7] Their use in a fully compatible CMOS technology context can unleash an overwhelming development of these applications to advance in neuromorphic computing and neural network hardware implementation.[3–7] Moreover, due to their inherent stochastic nature, these devices can

be used as entropy sources for cryptographic circuits, such as physical unclonable functions and random number generators.[8–10] RRAMs features allow us to stack cells in 3D and scale to very small process nodes. The cells typically employ a switching material (usually a transition metal oxide) sandwiched in between two metal electrodes.[1,2] One of the most important physical mechanisms associated with resistive switching (RS) is the formation and rupture of nanofilaments across the dielectric film. From a technology point of view, there is substantial flexibility to optimize the performance through an appropriate selection of switching materials and memory cell organization. However, although RRAMs have demonstrated some advantages over flash devices and other

emerging structures (phase change memories and ferroelectric memories) such as short read/write times, high endurance, low power operation, radiation hardness, CMOS compatibility, they are not exempt from serious drawbacks.[2,11] It is worth mentioning that massive industrial production still faces several challenges such as a high variability and the lack of reliable electronic design automation EDA tools. In this regard, compact models are essential tools to tackle these latter concerns.

RRAM compact modeling has been addressed in the last years at different levels. The Stanford model (STFM)[12–15] has been employed by many research groups. Other models have also been introduced.[16–20] In the general modeling context, both analytical expressions to describe device operation and parameter extraction techniques need to be developed as a whole.[21] Even well-established models are unable to reproduce certain observable phenomena and, therefore, they must be continuously improved to account for new physical and technological features associated with particular materials or devices. This is precisely the focus of our work. In particular, we take the intrinsic series resistance effect in RRAM operation analysis into consideration and report a systematic approach to extract this series resistance from the experimental results. As it will be shown in Secs. II–V, the role played by the series resistance is of utmost importance for understanding the RRAM electrical behavior, an issue which has been already recognized by several authors.[22–25] The study of the role played by the series resistance within RRAM models is particularly performed for the STFM since its use is extended and its algebraic formulation is both compact as well as intuitive. The enhanced STFM flexibility to reproduce valence change memories (VCM) experimental data is assessed in depth. For the sake of completeness, it is worth pointing out that in the last few years, VCM devices modeling has been addressed

following a variety of approaches;[12,14,16–18] in particular, different types of filament shapes have been considered (cylindrical, truncated cone, and hourglass[26]). In addition, from the analytical formulation viewpoint, the state variable has been assumed from a different perspective: the width of the gap between the conductive filament tip and the electrode,[12,13] the CF volume or radius,[17,18] and as a generalized memory variable.[27] The device current calculation has been performed also under different considerations including tunneling, Schottky, Poole–Frenkel, and ohmic conduction regimes.[12,14,20,26] Some of the modeling implementations also account for variability[28] and noise; in the latter case, Random Telegraph Noise (RTN) has been found appropriate for cryptographic purposes such as random number generation circuits.[9,29]

The paper is organized as follows, in Sec. II, we introduce the device fabrication and measurement details. Section III is devoted to the series resistance extraction procedures, while the modeling developments are tackled in Sec. IV, and finally, we wrap up with the main conclusions in Sec. V.

II. DEVICE DESCRIPTION AND MEASUREMENT

The RRAMs were fabricated using a highly doped N-type ($\rho = 4\,m\Omega\,cm$) silicon wafer. The top metal electrode consists of a 200 nm TiN/10 nm Ti bi-layer while the bottom metal, a 50 nm-thick W layer, was deposited on the silicon substrate with a 20 nm Ti adhesion layer, see Fig. 1(a). The back of the wafers was metalized with aluminum for electrically contacting the bottom electrode through the silicon substrate. The dielectric layer consists of a 10 nm-thick HfO_2 film deposited by ALD. The area of the devices is $15 \times 15\,\mu m^2$. It is worth mentioning that the fabricated RRAMs are valence change mechanism-based devices.
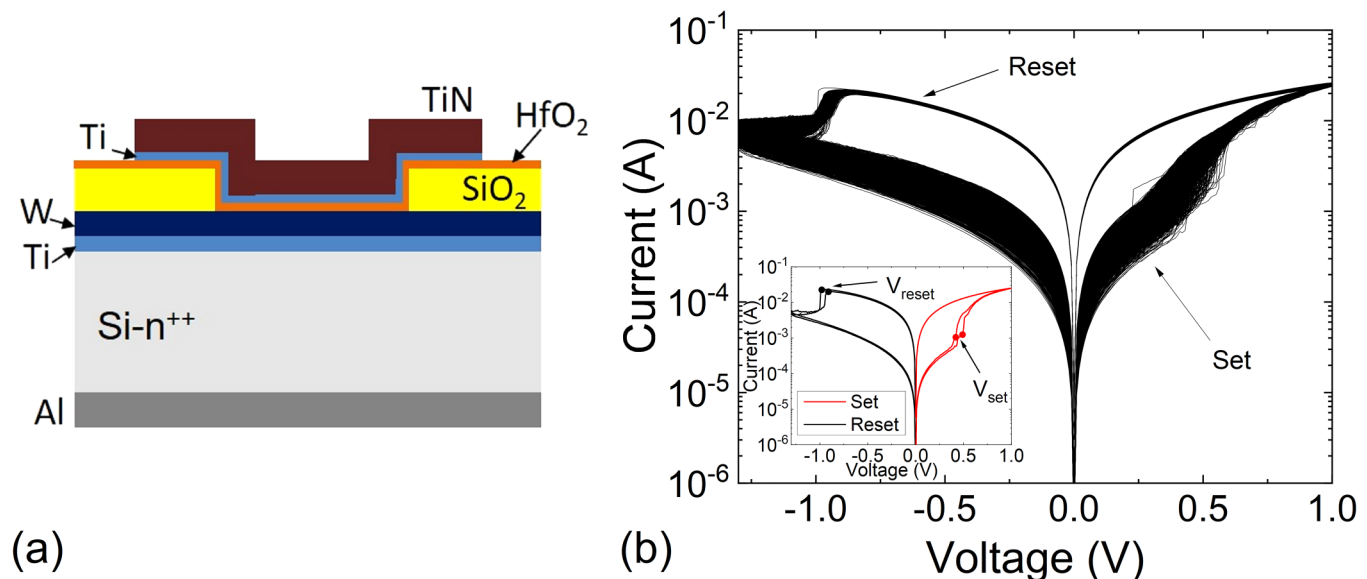

FIG. 1. (a) Layer stack scheme of the devices under study and (b) experimental I–V curves for 1000 set/reset cycles. The inset in (b) shows the set and reset voltages for two of the curves measured.
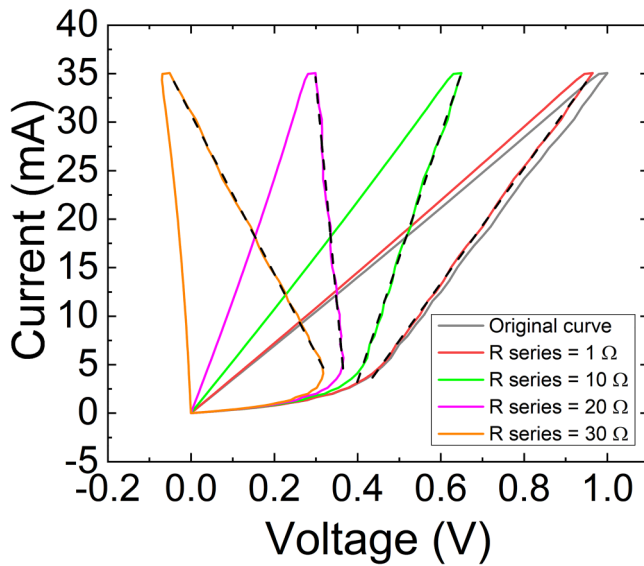
FIG. 2. Modified *I–V* curves (measured current vs V_N) for a set process making use of different series resistances. For the sake of clarity, only four curves corresponding to different series resistances are included. The black-dashed lines are the result of the linear regression performed to choose the curve with the highest slope in the methodology proposed.

The electrical characterization of the devices was performed applying a ramped voltage (0.08 V/s) to the TiN/Ti top electrode with a voltage step of 0.01 V and with the W bottom electrode grounded. A forming process was performed with current compliance $I_{CC} = 0.1$ mA and subsequently a sequence of 1000 RS cycles

was measured, see Fig. 1(b). These cycles consist of consecutive set and reset transitions. In particular, for positive voltages, a set process leads to the formation of a conductive filament (CF) that shorts the electrodes[30] and the device switches to the low resistance state (LRS). The reset process occurs at negative voltages, in this case, the CF is ruptured and the device switches back to the high resistance state (HRS).[30] See the set and reset voltages indicated in the inset of Fig. 1(b).

III. SERIES RESISTANCE AND TRANSITION VOLTAGES EXTRACTION

In order to calculate the intrinsic series resistance, R_{series}, for compact modeling purposes, a numerical procedure similar to that used in previous publications[22–24] is considered here. The method consists in using a redefined voltage scale, $V_N = V_{Applied} − I_{Measured} × R_{series}$, where $V_{Applied}$ is the external applied voltage and $I_{Measured}$ the measured current. We replot the experimental *I–V* curves (as the ones shown in Fig. 1) by changing the variable in the *X* axis to V_N instead of the experimental $V_{Applied}$. By sweeping R_{series}, we obtain different modified $I_{Measured}−V_N$ curves (see Fig. 2). Among them, we select the one with the steepest slope (close to a vertical line) in the region after the curve knee; in doing so, we make sure the set process is visualized properly as long as the current rises while the voltage is constant as shown in Fig. 2. This behavior is a clear sign of a sustained conductive filament growth that leads to a current rise even if the device voltage is fixed. The slope of the curve is computed by a linear regression scheme along its straightest part.

Based on the obtained R_{series} value, a comparison between V_{set} and the transition voltage for the set process (V_{TS}) is performed to assess the influence of R_{series} on the *I–V* curves. Notice that V_{set} is obtained from the original *I–V* curve (first point where the
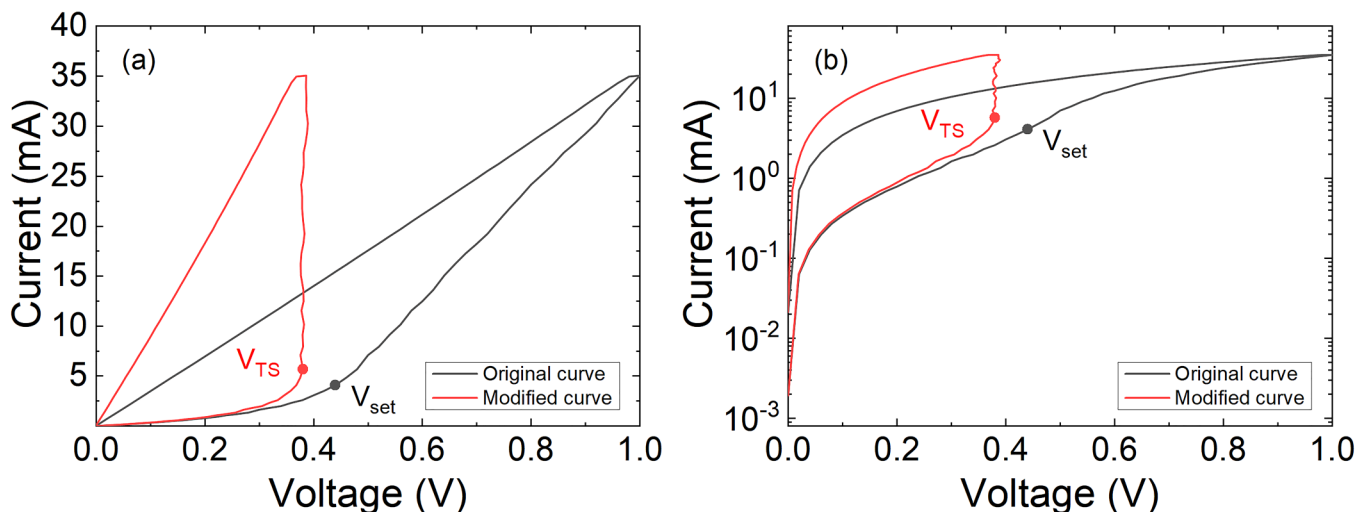

FIG. 3. Experimental current vs applied voltage for one cycle in a long RS series for one of the devices under study. The new transition voltage V_{TS} is obtained from the *I–V*_N curve. (a) Linear and (b) logarithmic scale.
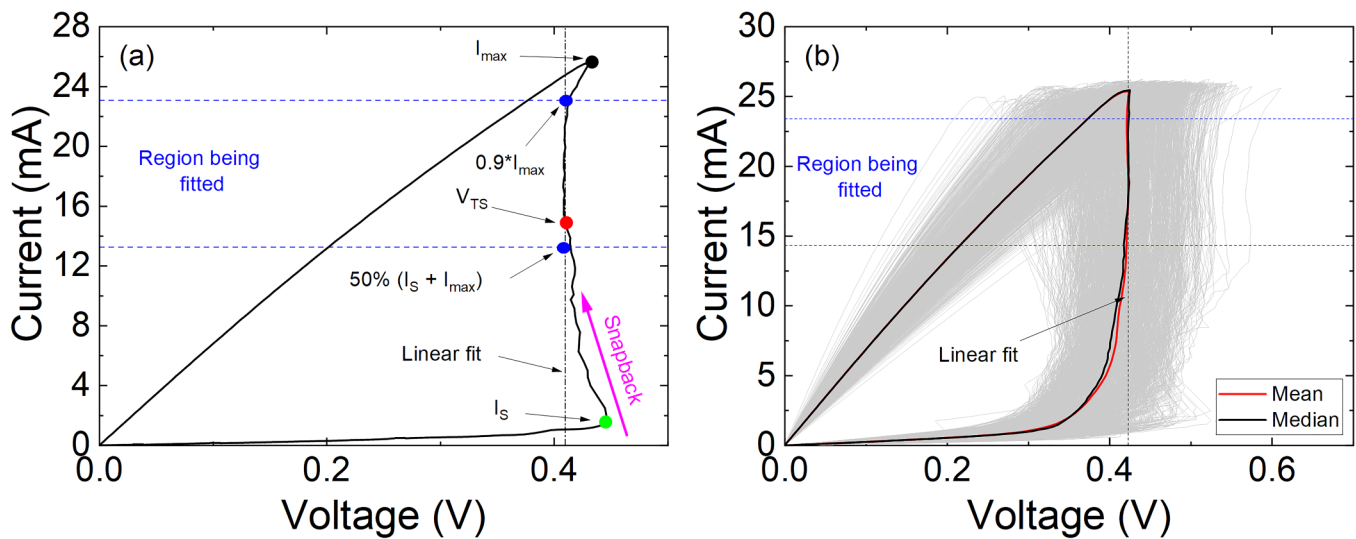
FIG. 4. (a) Modified I–V curve in a set process for a series resistance = 22.1 Ω. This value was obtained with the improved methodology. (b) Application of this methodology to the 1000 RS set cycles measured (for each I–V curve one series resistance value is obtained). The red line indicates the average curve (calculated as the mean) of all the RS cycles, while the black curve corresponds to the median curve of all the RS cycles considered.

maximum current slope along the I–V curve is found) and V_{TS} from the modified one ($I_{Measured}$–V_N) after the R_{series} calculation. In this latter case, the projection in the X axis of the vertical line obtained in the new curve ($I_{Measured}$–V_N) is assumed as V_{TS} (see Fig. 3).

The above described methodology can lead to erroneous values for the series resistance in some particular I–V_N curves (because of the snapback effect). In order to improve the

parameter extraction method, only a region of the vertical section of the modified I–V curve is fitted when searching for the steepest slope. As indicated in Fig. 4(a), the fitting region is selected to be in between a current value of $0.9 \times I_{max}$ and a current resulting from the average of the current (I_S) (obtained at the point where the set voltage is determined in the original experimental curve) and the maximum current I_{max}, as shown in Fig. 4(a). This
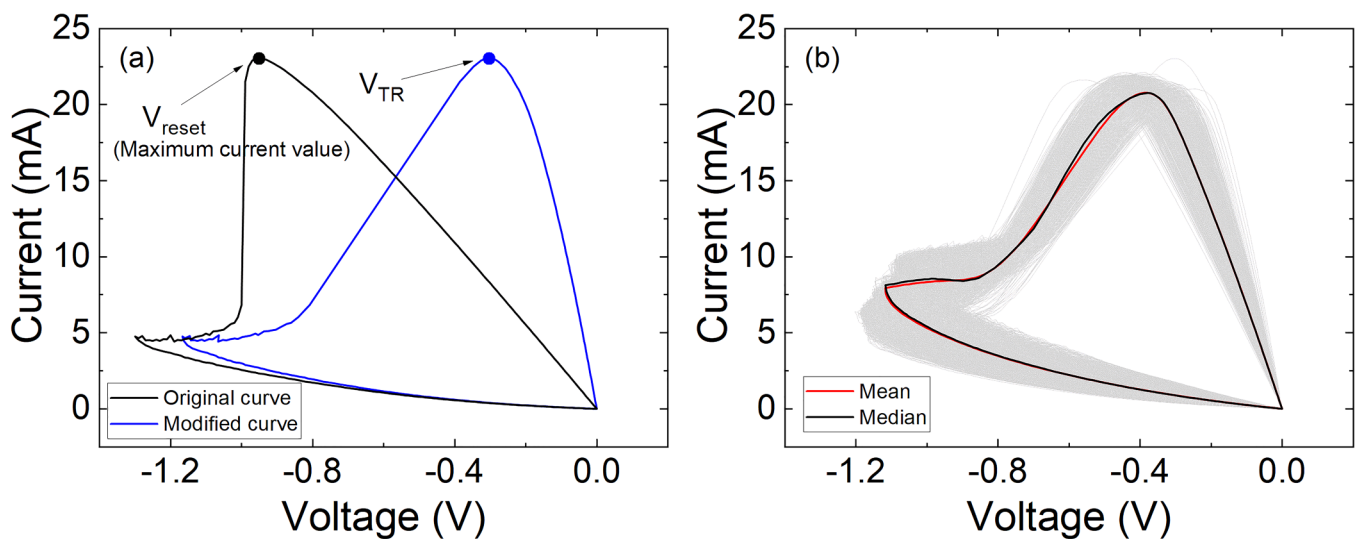

FIG. 5. (a) Experimental and modified reset I–V curves. (b) Modified I–V reset curves for the 1000 cycles measured. The red line corresponds to the average curve (calculated as the mean) of all the RS cycles and the black curve corresponds to the median.
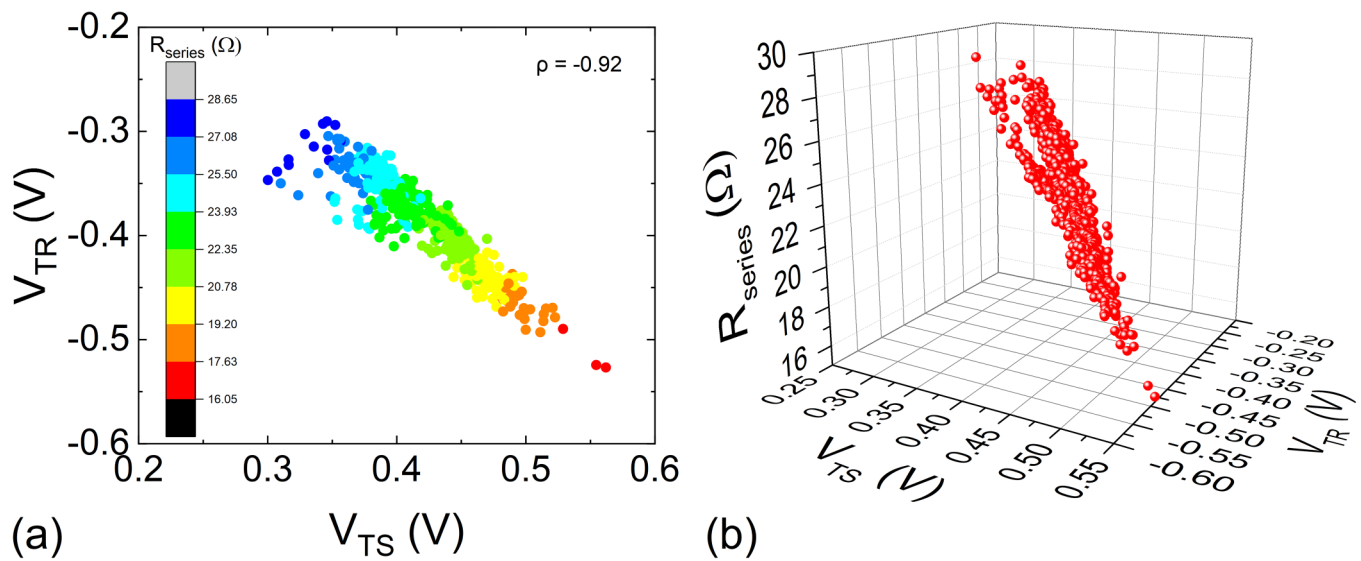
FIG. 6. Transition voltage for reset vs transition voltage for set for the data under study (1000 cycles). (a) The correlation of the variables plotted is shown and the corresponding series resistances are given in a color code. (b) 3D plot of the series resistance vs set transition voltage and reset transition voltage for the whole RS series.

methodology has been found to be more appropriate when snapback effects [Fig. 4(a)] take place in the lower part of the "intrinsic" $I–V$ curve.[22–24] By doing this, the snapback is avoided since this region represents the starting phase of the conductive filament formation (the weight of the series resistance with respect to the overall resistance, device plus series resistance, changes fast here). The proper set process takes place in the vertical section of the $I–V_N$ curve, as already stated. While the highest region of the curve cannot be considered because of a different reason. When the filament can no longer expand, the process slows down, which can be regarded as the appearance of an additional series resistance.

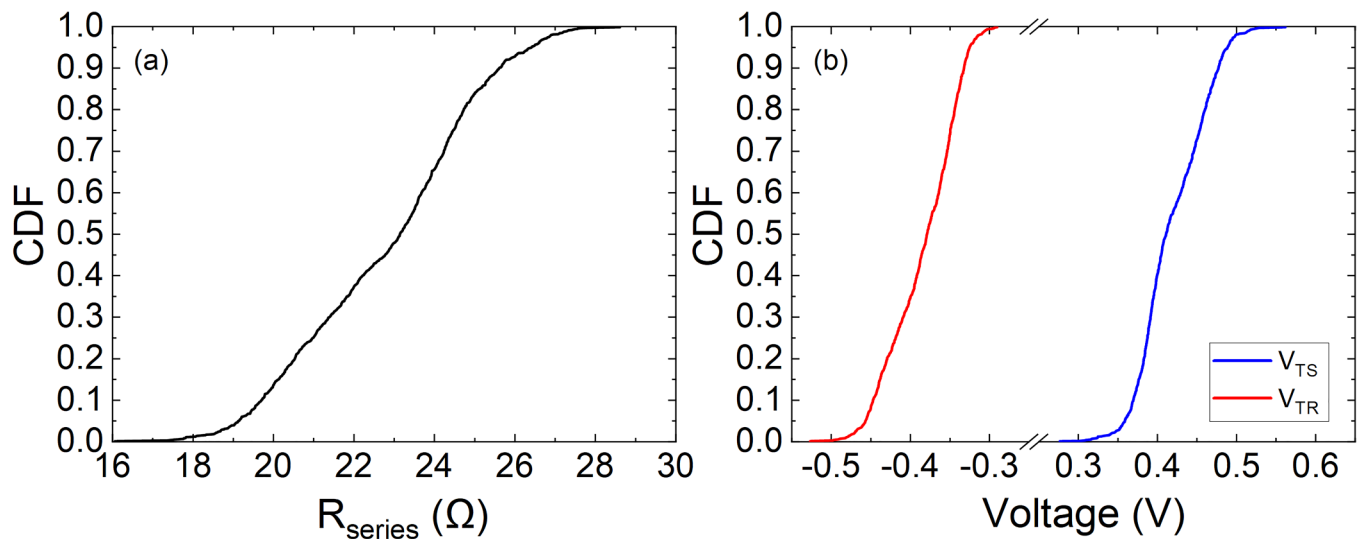**FIG. 7.** Cumulative distribution functions for the studied parameters in the whole RS series: (a) series resistance and (b) transition voltages for the set (V_{TS}) and for the reset processes (V_{TR}). The mean values for the series resistance, V_{TS}, and V_{TR} are 22.80 Ω, 0.418 V, and −0.384 V, respectively. The standard deviation for the latter parameters is 2.26 Ω, 0.042 V, and 0.043 V in each case.
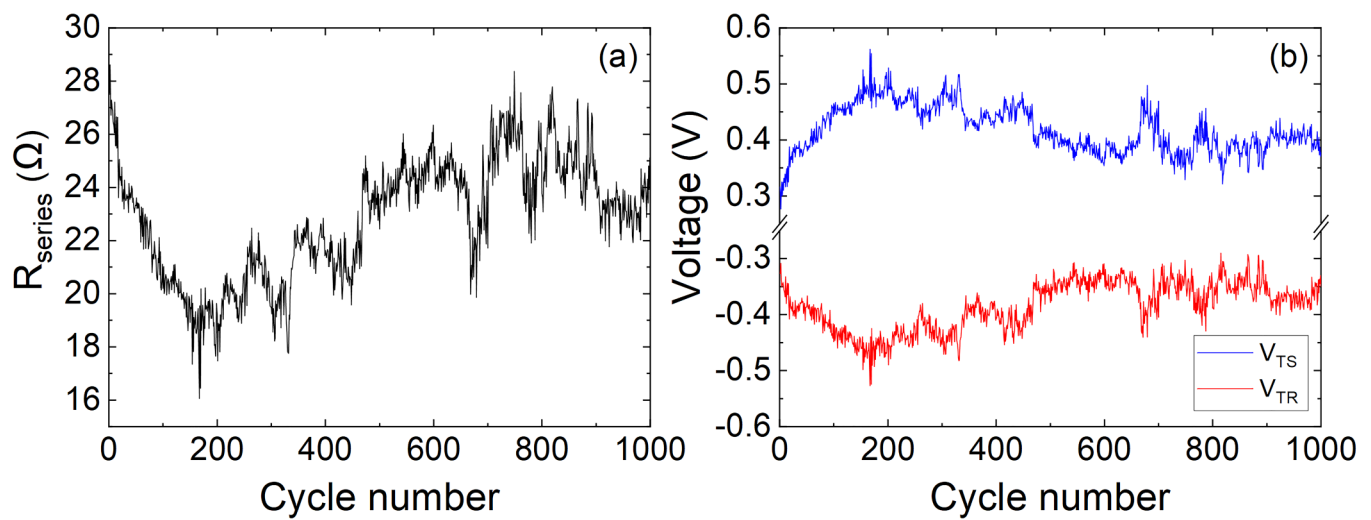
FIG. 8. (a) Calculated series resistance vs cycle number in the whole RS series for the data under study and (b) set transition voltage (V_{TS}) and reset transition voltage (V_{TR}) vs cycle number in the whole RS series for the data under study.
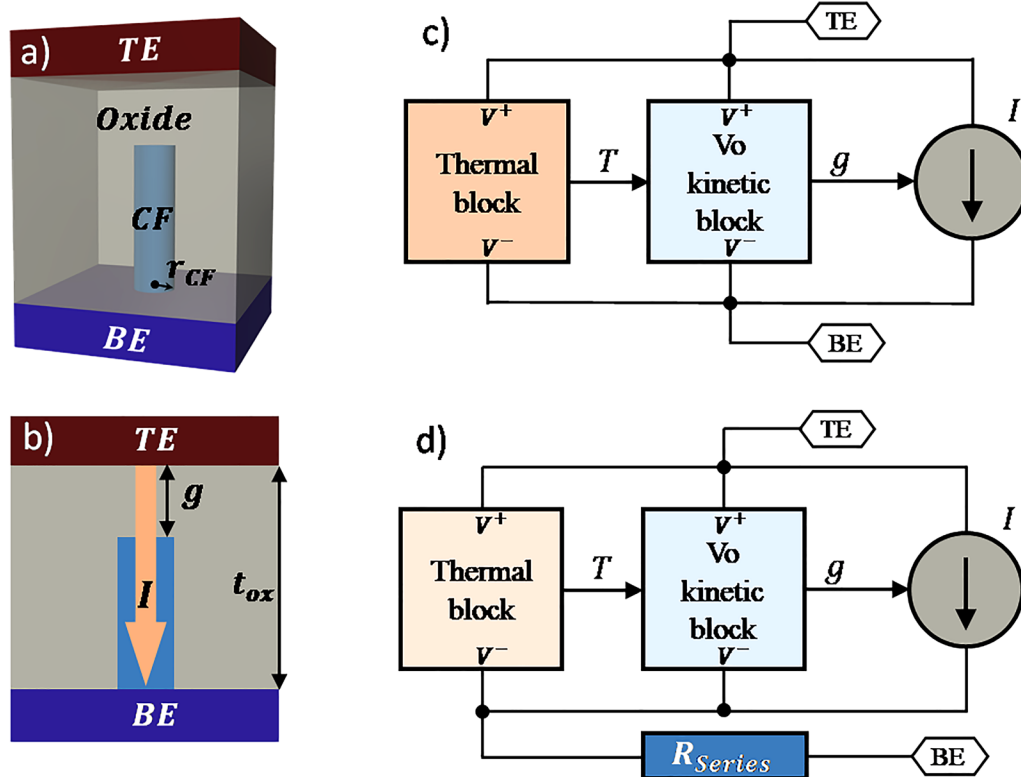
FIG. 9. (a) Three-dimensional view of the STFM modeling structure with an indication of different device regions [top electrode (TE), dielectric, conductive filament, and bottom electrode (BE)] and (b) schematic representation of the main model geometrical parameters. The gap (g) between the TE and the filament tip is one of the state variables, the other one is the temperature (T), (c) subcircuit for the STFM implementation, and (d) proposed modification of STFM implementation with cylindrical CF including the series resistance.

FIG. 10. Experimental (black symbols) and modified current (red symbols) vs voltage. Modeled data employing the STFM are shown for the modified (red line) and original (black line, in this case, it is included an external resistance to account for the role of the series resistance, see the schematic). (a) Linear and (b) logarithmic scales.

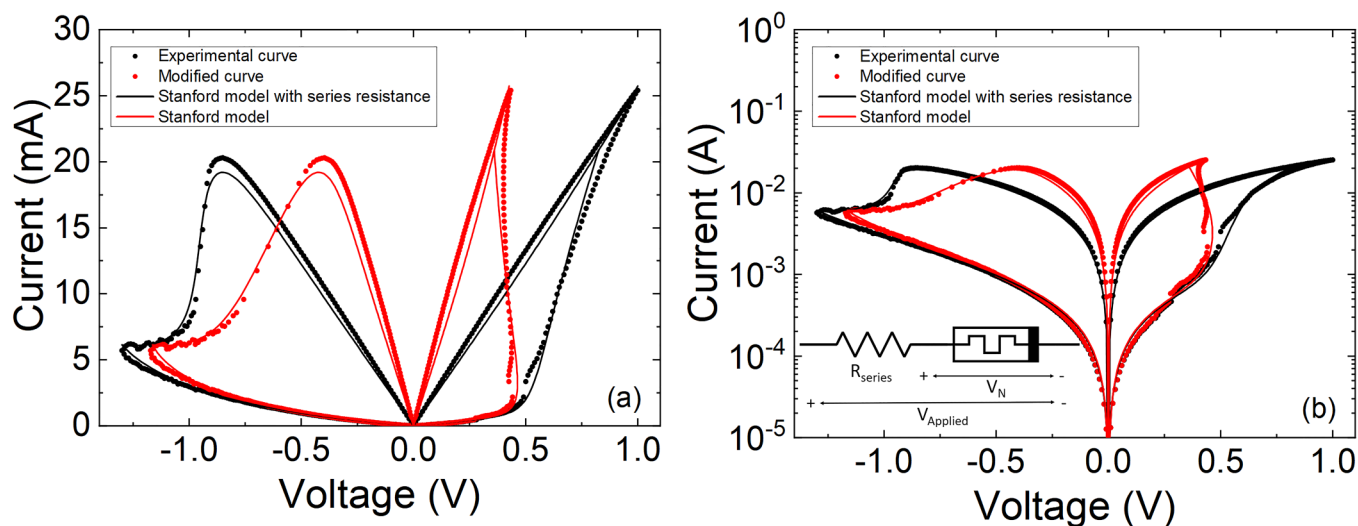Figure 4(b) shows the proposed fitting methodology applied to the measured 1000 RS cycles as well as the median and average I–V curve. As it can be seen, the snapback effect is clear for some of the curves plotted. Once R_{series} is determined after obtaining the steepest slope, the reset curves are corrected accordingly as illustrated in Fig. 5.

In addition, the reset and reset transition (V_{TR}) voltages are calculated from the measured and corrected reset curves, respectively. They are obtained as the voltages corresponding to the maximum current values, see Fig. 5(a). Notice that the values of the set and reset transition voltages are quite similar, suggesting a clear electric field dependence of the resistive switching mechanisms. They are the minimum voltages required to induce the vacancy movements in opposite directions. Nevertheless, temperature effects are also known to be involved in resistive switching due to the thermally activated nature of the diffusive transport mechanism.[12,30–35] It is interesting to notice the axes scale in Fig. 6(a), the transition voltages are located in relatively narrow intervals; i.e., cycle-to-cycle variability is low (within a few tenths of a volt). In addition, see that the higher the transition voltages absolute value, the lower the series resistance, Fig. 6(b).

Figure 7(a) illustrates the cumulative distribution function (CDF) for the series resistances extracted from the 1000 cycles measured. The corresponding transition voltages CDFs are shown in Fig. 7(b). Notice that V_{TS} and V_{TR} are described by the same CDF except for the voltage sign (they are parallel).

The variability of the series resistance and the transition voltages as a function of the cycle number is illustrated in Figs. 8(a) and 8(b), respectively. A reasonable modeling of these numerical series can be performed by means of time series analysis for circuit simulation purposes.[36] Notice that cycle-to-cycle (C2C) autocorrelation effects cannot be disregarded. In addition, the results seem to be consistent, at least in the medium term, with a mean-reverting stochastic process. In the case of V_{TR} and V_{TS}, the cross-correlation is more than evident: as V_{TS} increases, V_{TR} decreases in a symmetrical fashion. Again, this is a clear evidence that the same physical mechanism activates the switching process.

Once the intrinsic series resistance parameter is extracted, the C2C variability and the statistical distribution of the results can be analyzed and quantified; in Sec. IV, we introduce the observed parameter variation in the compact modeling approach. It is important to highlight that the methodology introduced here, although presented for VCM devices could also be employed with other RRAM technologies.

IV. SERIES RESISTANCE INFLUENCE ON RRAM COMPACT MODELING

In this section, the role played by the series resistance in the RRAM electrical behavior is investigated by means of the Stanford

TABLE I. Stanford model parameters employed for the fitting of the experimental devices under study, in particular, for the cycle selected in Fig. 10.

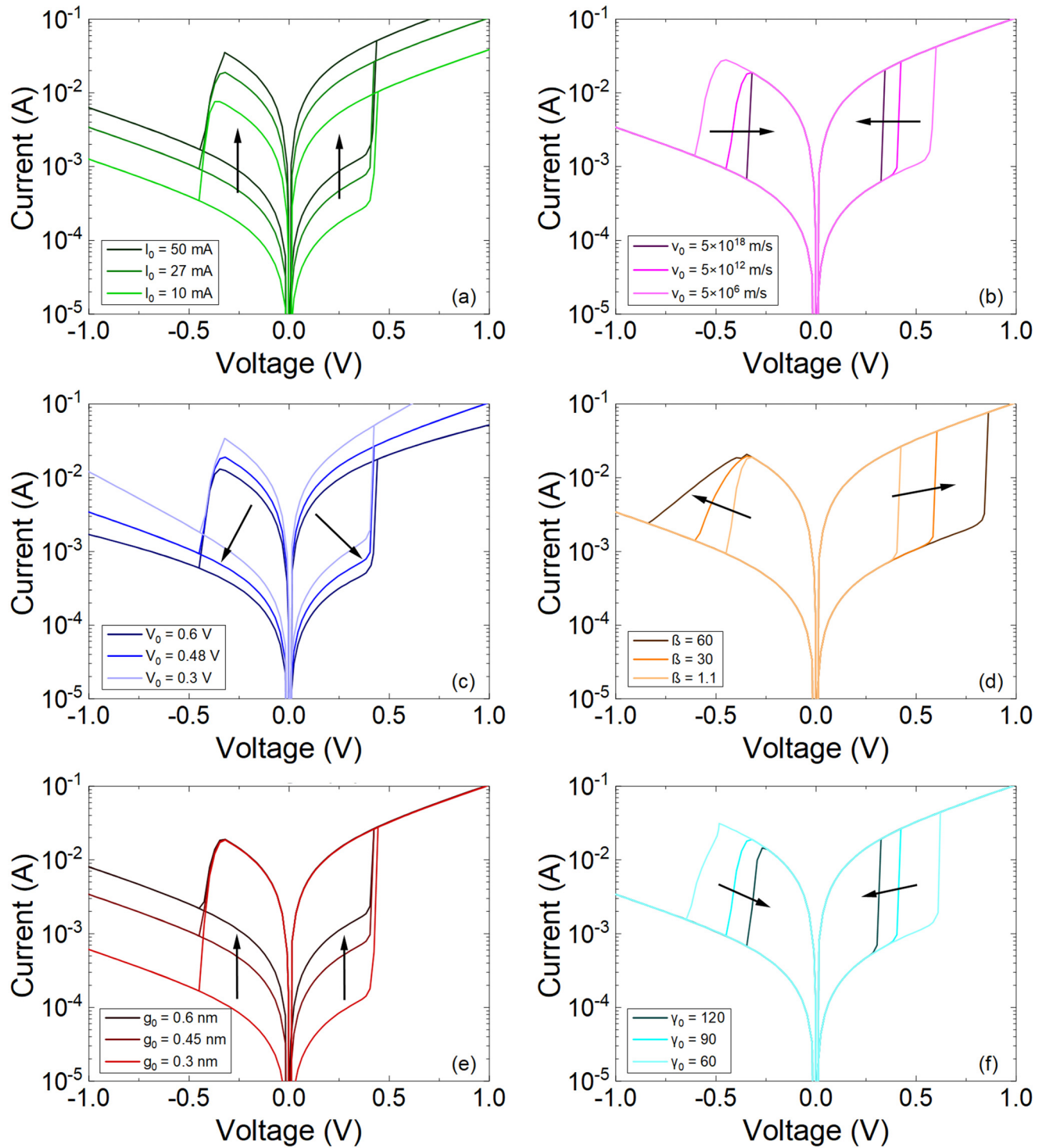| Stanford model parameters			
Device parameters	Unit	Resistive switching	
		Set	Reset
V_o	V	0.45	
I_0	mA	48	
g_0	nm	0.35	
v_0	m/s	5×10^6	
A	...	1	1.1
B	...	1	15
γ_0	...	20	

FIG. 11. Current vs voltage for the modeled curves obtained with the Stanford model isolating some parameter variations. (a) I_0, (b) v_0, (c) V_0, (d) β, (e) g_0, and (f) γ_0.

model,[12–15] see Fig. 9. The model consists in a differential equation that describes the gap between the conductive filament tip and the electrode (g), a current equation that shows exponential dependencies with the gap and the applied voltage and a thermal model that allows the calculation of the main filament temperature by means of the device thermal resistance and capacitance. The series resistance is introduced as a series component to the original model. Notice that by doing this we consider the case in which part of this series resistance can be external to the device.

Figure 10 illustrates a typical RS cycle simulation using the STFM. The model is coded in Verilog-A. The inclusion of the series resistance notably improves the fitting of the original experimental results (see Table I for the model parameters).

The fitting was performed with and without a series resistance (previously extracted, $R_{series} = 22.3\,\Omega$) in the simulation, see Fig. 9(d). As can be seen, a good approximation was obtained in

the experimental I–V curve. This versatile and simple model works well; however, for higher accuracy, other models (with even higher complexity) need to be considered.[16–19] As expected, there is a trade-off between accuracy and complexity in the RRAM modeling approach. In particular, for the devices considered here, we assume some model parameters different for the set and reset processes, as suggested in Ref. 14, see Table I.

Importantly, the set of parameters employed to simulate the TiN/Ti/HfO$_2$/W structure is different from what was used for other type of devices.[14] In particular, device currents for our devices are higher than those reported in Ref. 14 and the abruptness of the I–V curves at the onset of the set and reset processes is different. To have a clear picture of the model behavior, we have analyzed the influence of some of the model parameters on the I–V curve shape, see Fig. 11 (in this case, no series resistance correction is included). By accounting for the parameter variation, we can reproduce the

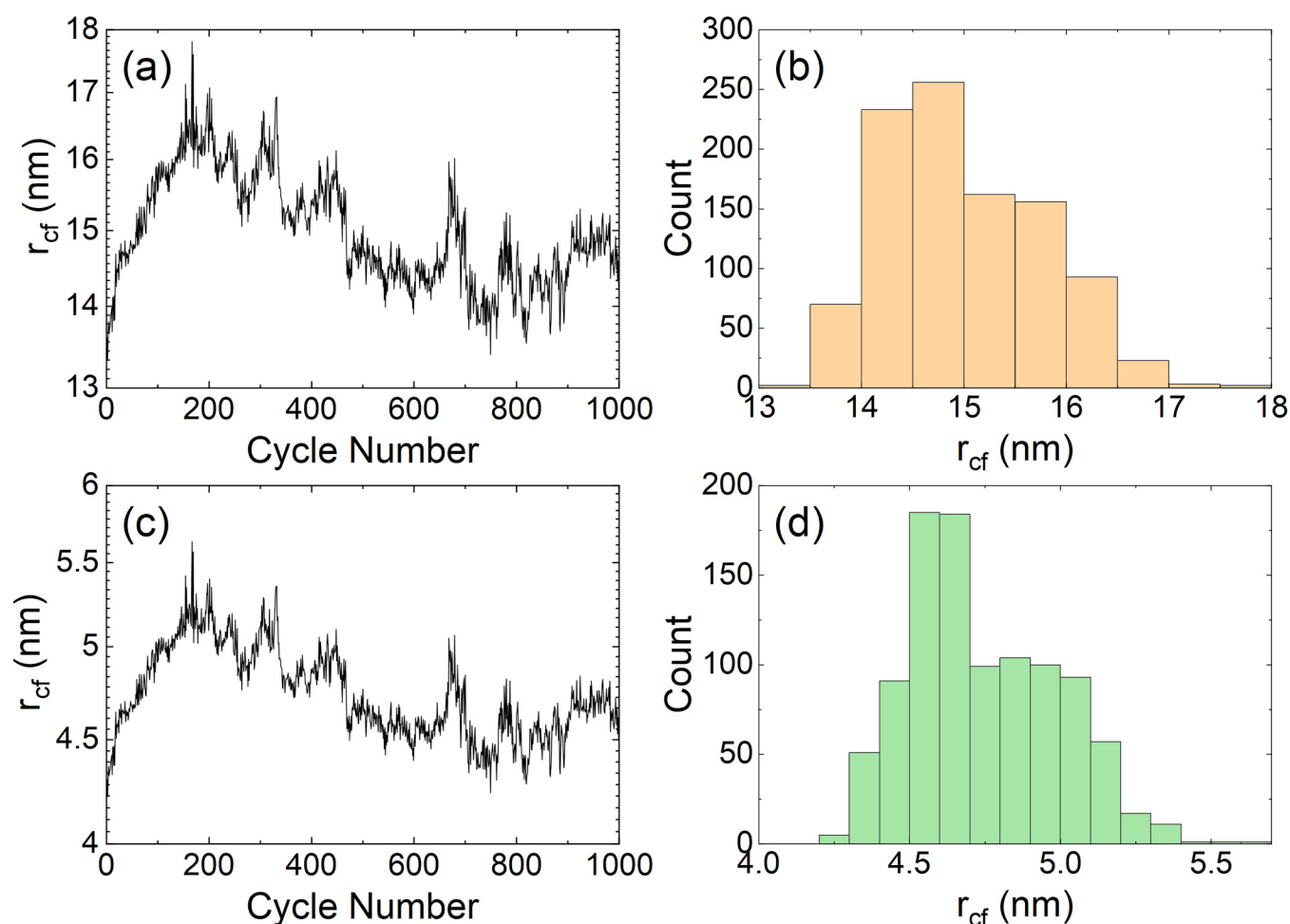**FIG. 12.** Calculated radii of a cylindrical CF employed to model series resistance vs cycle number in the whole RS series obtained considering $g = 2\,nm$ and $\sigma_{CF} = 5 \times 10^5\,S/m$ (a) or $g = 2\,nm$ and $\sigma_{CF} = 5 \times 10^6\,S/m$ (c). (b) and (d) Corresponding cylinder radii histogram for $g = 2\,nm$ and $\sigma_{CF} = 5 \times 10^5\,S/m$ ($\sigma_{CF} = 5 \times 10^6\,S/m$).
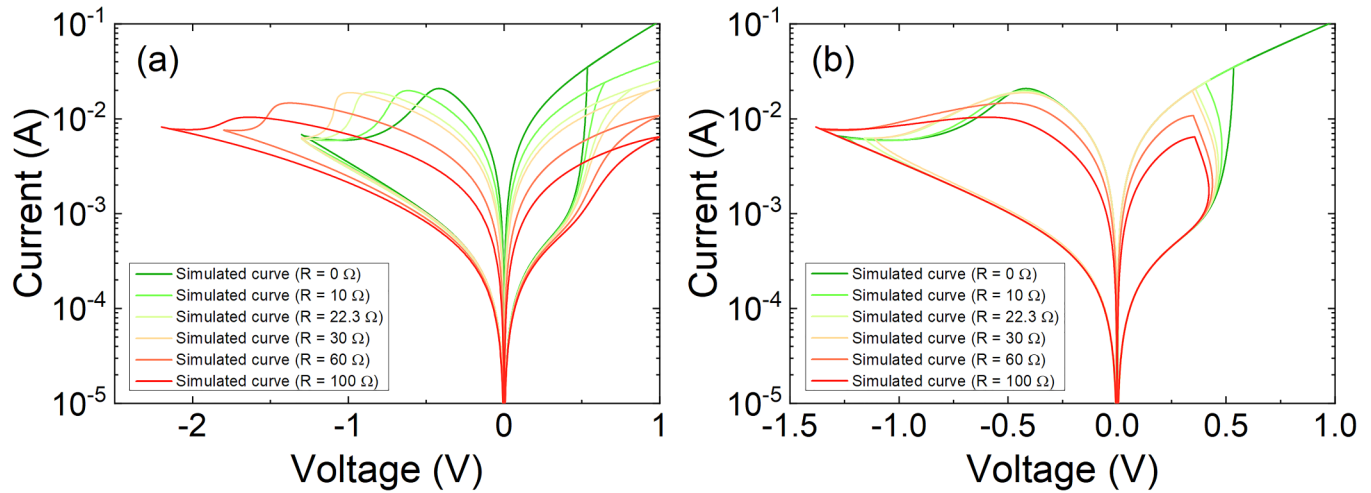
FIG. 13. Modeled current vs voltage curves for different series resistances. (a) Current vs RRAM applied voltage (I–$V_{Applied}$). (b) Current vs modified voltage (I–V_N) using the series resistances.

cycle-to-cycle variability observed in our devices. Although this is out of the scope of this paper, we will try to establish next the connection between the resistance variation and the CF physical aspect.

In order to complete the picture, the series resistance effect can be incorporated into the STFM assuming approximately a cylinder-like structure for the CF. This could be linked to the filament remnants after the reset process. In this case, as shown in the schematics included in Fig. 9, due to the particularities of these devices, we can compute the cylinder radius under this approximation using Eq. (1) (see Fig. 12),

$$R_{series} = \frac{t_{ox} - g}{\pi \sigma_{CF} r_{CF}^2}.$$ (1)

The following values for the gap and electrical conductivity are considered in Figs. 12(a) and 12(b) (g = 2 nm and σ_{CF} = 5 × 10⁵ S/m, this latter value is in line with those previous reported in Ref. 17), and in Figs. 12(c) and 12(d), g = 2 nm and σ_{CF} = 5 × 10⁶ S/m (a conductivity value in line with Ref. 37) were employed.

See that the estimated radii are in the order of several nanometers [Figs. 12(a) and 12(b)] but recall that this could depend on the electrical conductivity considered [Figs. 12(c) and 12(d)]; in this respect, a kind of "effective" radii should be understood here since, in real devices, conductive filaments are not strictly cylindrical; in fact, the wider parts seem to be located close to the electrodes.[30]

Finally, Fig. 13 shows the original fitting (see the red line in Fig. 10) and simulations including a series resistance ranging from 0 to 100 Ω. The role played by the series resistance is clearly recognized from these plots. The experimental I–V curve shapes in this type of devices (Fig. 1) are more closely reproduced when series resistances are included (Fig. 13). In particular, as the series

resistance increases the set curve slope drops off. Notice that this is not related to the progressiveness of the set transition but only a consequence of the additional potential drop. Similarly, a more progressive current reduction in the reset region is seen as the series resistance increases.

V. CONCLUSIONS

The role played by the intrinsic series resistance in RRAM devices has been analyzed from a compact modeling viewpoint. The extraction procedure of the series resistance parameter has been evaluated using experimental data from HfO₂-based VCM devices. The use of the series resistance to redefine the measured I–V curves allows us to extract device transition voltages. These transition voltages are shown to be correlated. It has been found that the lower the series resistance is, the higher the transition voltage absolute values are. We have also employed the series resistance to enhance the accuracy of the RRAM Stanford model. The use of this parameter to enhance the Stanford model allows us to improve experimental data fitting.

ACKNOWLEDGMENTS

DATA AVAILABILITY

The data that support the findings of this study are available from the corresponding author upon reasonable request.

REFERENCES

[1]M. Lanza, H.-S. P. Wong, E. Pop, D. Ielmini, D. Strukov, B. C. Regan, L. Larcher, M. A. Villena, J. J. Yang, L. Goux, A. Belmonte, Y. Yang, F. M. Puglisi, J. Kang, B. Magyari-Köpe, E. Yalon, A. Kenyon, M. Buckwell, A. Mehonic, A. Shluger, H. Li, T.-H. Hou, B. Hudec, D. Akinwande, R. Ge, S. Ambrogio, J. B. Roldan, E. Miranda, J. Suñé, K. L. Pey, X. Wu, N. Raghavan, E. Wu, W. D. Lu, G. Navarro, W. Zhang, H. Wu, R. Li, A. Holleitner, U. Wurstbauer, M. Lemme, M. Liu, S. Long, Q. Liu, H. Lv, A. Padovani, P. Pavan, I. Valov, X. Jing, T. Han, K. Zhu, S. Chen, F. Hui, and Y. Shi, "Recommended methods to study resistive switching devices," Adv. Electron. Mater. **5**, 1800143 (2019).

[2]F. Pan, S. Gao, C. Chen, C. Song, and F. Zeng, "Recent progress in resistive random access memories: Materials, switching mechanisms and performance," Mater. Sci. Eng. R Rep. **83**, 1–59 (2014).

[3]Z. Wang, C. Li, W. Song, M. Rao, D. Belkin, Y. Li, P. Yan, H. Jiang, P. Lin, M. Hu, J. P. Strachan, N. Ge, M. Barnell, Q. Wu, A. G. Barto, Q. Qiu, R. S. Williams, Q. Xia, and J. J. Yang, "Reinforcement learning with analogue memristor arrays," Nat. Electron. **2**, 115–124 (2019).

[4]P. Yao, H. Wu, B. Gao, J. Tang, Q. Zhang, W. Zhang, J. J. Yang, and H. Qian, "Fully hardware-implemented memristor convolutional neural network," Nature **577**, 641–646 (2020).

[5]P. A. Merolla, J. V. Arthur, R. Alvarez-Icaza, A. S. Cassidy, J. Sawada, F. Akopyan, B. L. Jackson, N. Imam, C. Guo, Y. Nakamura, B. Brezzo, I. Vo, S. K. Esser, R. Appuswamy, B. Taba, A. Amir, M. D. Flickner, W. P. Risk, R. Manohar, and D. S. Modha, "A million spiking-neuron integrated circuit with a scalable communication network and interface," Science **345**, 668–673 (2014).

[6]F. Alibart, E. Zamanidoost, and D. B. Strukov, "Pattern classification by memristive crossbar circuits using *ex situ* and *in situ* training," Nat. Commun. **4**, 2072 (2013).

[7]M. Prezioso, F. Merrikh-Bayat, B. D. Hoskins, G. C. Adam, K. K. Likharev, and D. B. Strukov, "Training and operation of an integrated neuromorphic network based on metal-oxide memristors," Nature **521**, 61–64 (2015).

[8]R. Carboni and D. Ielmini, "Stochastic memory devices for security and computing," Adv. Electron. Mater. **5**, 1900198 (2019).

[9]M. Lanza, C. Wen, X. Li, T. Zanotti, F. M. Puglisi, Y. Shi, F. Saiz, A. Antidormi, S. Roche, W. Zheng, X. Liang, J. Hu, S. Duhm, K. Zhu, F. Hui, J. B. Roldan, B. Garrido, T. Wu, V. Chen, and E. Pop, "Advanced data encryption using two-dimensional materials," Adv. Mater. **33**, 2100185 (2021).

[10]D. Arumí, S. Manich, R. Rodríguez-Montañés, and M. Pehl, "RRAM based random bit generation for hardware security applications," in *2016 Conference on Design of Circuits and Integrated Systems (DCIS), Granada* (IEEE, 2016), pp. 1–6.

[11]M. A. Zidan, J. P. Strachan, and W. D. Lu, "The future of electronics based on memristive systems," Nat. Electron. **1**, 22–29 (2018).

[12]X. Guan, S. Yu, and H.-S. Philip Wong, "A SPICE compact model of metal oxide resistive switching memory with variations," IEEE Electron Device Lett. **33**(10), 1405–1407 (2012).

[13]Z. Jiang, S. Yu, Y. Wu, J. H. Engel, X. Guan, and H. S. P. Wong, "Verilog-A compact model for oxide-based resistive random access memory," in *2014 International Conference on Simulation of Semiconductor Processes and Devices (SISPAD), 9–11 September* (IEEE, 2014), pp. 41–44.

[14]Z. Jiang, Y. Wu, S. Yu, L. Yang, K. Song, Z. Karim, and H.-S. P. Wong, "A compact model for metal–oxide resistive random access memory with experi- mental verification," IEEE Trans. Electron Devices **63**(5), 1884–1892 (2016).

[15]P.-Y. Chen and S. Yu, "Compact modeling of RRAM devices and its applica- tions in 1T1R and 1S1R array design," IEEE Trans. Electron Devices **62**(12), 4022–4028 (2015).

[16]P. Huang, X. Y. Liu, B. Chen, H. T. Li, Y. J. Wang, Y. X. Deng, and J. F. Kang, "A physics-based compact model of metal-oxide-based RRAM DC and AC oper- ations," IEEE Trans. Electron Devices **60**(12), 4090–4097 (2013).

[17]G. González-Cordero, F. Jiménez-Molinos, J. B. Roldán, M. B. González, and F. Campabadal, "An in-depth study of the physics behind resistive switching in TiN/Ti/HfO2/W structures," J. Vac. Sci. Technol. B **35**, 01A110 (2017).

[18]G. González-Cordero, M. B. González, H. García, F. Campabadal, S. Dueñas, H. Castán, F. Jiménez-Molinos, and J. B. Roldán, "A physically based model for resistive memories including a detailed temperature and variability description," Microelectron. Eng. **178**, 26–29 (2017).

[19]P. Huang, D. Zhu, S. Chen, Z. Zhou, Z. Chen, B. Gao, and J. Kang, "Compact model of HfOX-based electronic synaptic devices for neuromorphic computing," IEEE Trans. Electron Devices **64**(2), 614–621 (2017).

[20]M. A. Villena, J. B. Roldán, F. Jiménez-Molinos, E. Miranda, J. Suñé, and M. Lanza, "SIM2RRAM: A physical model for RRAM devices simulation," J. Comput. Electron. **16**, 1095 (2017).

[21]R. Woltjer, L. Tiemeijer, and D. Klaassen, "An industrial view on compact modeling," Solid State Electron. **51**, 1572–1580 (2007).

[22]V. Karpov, D. Niraula, and I. Karpov, "Thermodynamic analysis of conductive filaments," Appl. Phys. Lett. **109**, 093501 (2016).

[23]D. J. Wouters, S. Menzel, J. A. J. Rupp, T. Hennen, and R. Waser, "On the uni- versality of the I–V switching characteristics in non-volatile and volatile resistive switching oxides," Faraday Discuss. **213**, 183–196 (2018).

[24]A. Fantini, D. J. Wouters, R. Degraeve, L. Goux, L. Pantisano, G. Kar, Y.-Y. Chen, B. Govoreanu, J. A. Kittl, L. Altimime, and M. Jurczak, "Intrinsic switching behavior in HfO2 RRAM by fast electrical measurements on novel 2R test structures," in *4th IEEE International Memory Workshop, Milan* (IEEE, 2012), pp. 1–4.

[25]M. B. González, M. Maestro, F. Jiménez-Molinos, J. B. Roldán, and F. Campabadal, "Current transient response and role of the internal resistance in HfOx-based memristors," Appl. Phys. Lett. **117**, 262902 (2020).

[26]R. Degraeve, A. Fantini, N. Raghavan, L. Goux, S. Clima, Y. Y. Chen, A. Belmonte, S. Cosemans, B. Goroveanu, D. J. Wouters, Ph. Roussel, G. S. Kar, G. Groeseneken, and M. Jurczak, "Hourglass concept for RRAM: A dynamic and statistical device model," in *Proceedings of the 21th International Symposium on the Physical and Failure Analysis of Integrated Circuits (IPFA)* (IEEE, 2014), pp. 245–249.

[27]E. Miranda and J. Suñé, "Memristive state equation for bipolar resistive switch- ing devices based on a dynamic balance model and its equivalent circuit repre- sentation," IEEE Trans. Nanotechnol. **19**, 837–840 (2020).

[28]E. Salvador, M. B. Gonzalez, F. Campabadal, J. Martin-Martinez, R. Rodriguez, and E. Miranda, "SPICE modeling of cycle-to-cycle variability in RRAM devices," Solid State Electron. **185**, 108040 (2021).

[29]G. González-Cordero, M. B. González, F. Campabadal, F. Jiménez-Molinos, and J. B. Roldán, "A physically based SPICE model for RRAMs including RTN," in *2020 XXXV Conference on Design of Circuits and Integrated Systems (DCIS)* (IEEE, 2020), pp. 1–6.

[30]S. Aldana, P. García-Fernández, R. Romero-Zaliz, M. B. González, F. Jiménez-Molinos, F. Gómez-Campos, F. Campabadal, and J. B. Roldán, "Resistive switching in HfO2 based valence change memories, a comprehen- sive 3D kinetic Monte Carlo approach," J. Phys. D: Appl. Phys. **53**, 225106 (2020).

[31]S. Aldana, P. García-Fernández, A. Rodríguez-Fernández, R. Romero-Zaliz, M. B. González, F. Jiménez-Molinos, F. Campabadal, F. Gómez-Campos, and J. B. Roldán, "A 3D kinetic Monte Carlo simulation study of resistive switching processes in Ni/HfO2/Si-n+-based RRAMs," J. Phys. D: Appl. Phys. **50**, 335103 (2017).

[32]S. Menzel, P. Kaupmann, and R. Waser, "Understanding filamentary growth in electrochemical metallization memory cells using kinetic Monte Carlo simula- tions," Nanoscale **7**, 12673 (2015).

[33]A. Padovani, L. Larcher, O. Pirrotta, L. Vandelli, and G. Bersuker, "Microscopic modeling of HfOx RRAM operations: From forming to switching," IEEE Trans. Electron Devices **62**(6), 1998–2006 (2015).

[34]S. Dirkmann, J. Kaiser, C. Wenger, and T. Mussenbrock, "Filament growth and resistive switching in hafnium oxide memristive devices," ACS Appl. Mater. Interfaces **10**(17), 14857–14868 (2018).

[35]M. Maestro, M. B. González, F. Jiménez-Molinos, E. Moreno, J. B. Roldán, and F. Campabadal, "Unipolar resistive switching behavior in Al_2O_3/HfO_2 multilayer dielectric stacks: Fabrication, characterization and simulation," Nanotechnology **31**, 135202 (2020).

[36]J. B. Roldán, F. J. Alonso, A. M. Aguilera, D. Maldonado, and M. Lanza, "Time series statistical analysis: A powerful tool to evaluate the variability of resistive switching memories," J. Appl. Phys. **125**, 174504 (2019).

[37]M. Bocquet, D. Deleruyelle, H. Aziza, C. Muller, J.-M. Portal, T. Cabout, and E. Jalaguier, "Robust compact model for bipolar oxide-based resistive switching memories," IEEE Trans. Electron Devices **61**, 674–681 (2014).